Minimal Models for Nonreciprocal Amplification Using Biharmonic Drives

A. Kamal[1,2] and A. Metelmann[3]
[1]Department of Physics and Applied Physics, University of Massachusetts, Lowell, Massachusetts 01854, USA
[2]Research Laboratory of Electronics, Massachusetts Institute of Technology, Cambridge, Massachusetts 02139, USA
[3]Department of Electrical Engineering, Princeton University, Princeton, New Jersey 08544, USA
(Received 28 August 2016; revised manuscript received 25 January 2017; published 28 March 2017)

We present a generic system of three bosonic modes coupled parametrically with a time-varying coupling modulated by a combination of two pump harmonics, and we show how this system provides the minimal platform for realizing nonreciprocal couplings that can lead to gainless photon circulation, and phase-preserving or phase-sensitive directional amplification. Explicit frequency-dependent calculations within this minimal paradigm highlight the separation of amplification and directionality bandwidths, a feature generic to such schemes. We also study the influence of counterrotating interactions that can adversely affect directionality and the associated bandwidth; we find that these effects can be mitigated by suitably designing the properties of the auxiliary mode that plays the role of an engineered reservoir to the amplification mode space.

DOI: 10.1103/PhysRevApplied.7.034031

I. INTRODUCTION

Quantum-limited detectors and amplifiers are important modules for practical quantum-information architectures. High-efficiency signal processing implemented with these systems has enabled single-shot readout [1] and real-time feedback control [2] of quantum bits in recent times. Quantum-limited detection is intimately tied to the minimality of the mode space of amplification, as each additional mode introduced into the system potentially brings along its associated noise, the minimum being the quantum-noise or zero-point fluctuations of the mode. Parametric systems achieve quantum-limited amplification by splitting a pump photon(s) between two channels, the (desired) signal and the (auxiliary) idler, a process which leads to the well-known quantum limit of half a photon of added noise at the signal frequency [3]. Such amplification, in general, is described as a scattering between input and output signal and idler field amplitudes $a_{\mathrm{sig,idl}}$,

$$\begin{pmatrix} a_{\mathrm{sig}} \\ a_{\mathrm{idl}} \end{pmatrix}^{\mathrm{out}} = \begin{pmatrix} \sqrt{\mathcal{G}+1} & \sqrt{\mathcal{G}} \\ \sqrt{\mathcal{G}} & \sqrt{\mathcal{G}+1} \end{pmatrix} \begin{pmatrix} a_{\mathrm{sig}} \\ a_{\mathrm{idl}} \end{pmatrix}^{\mathrm{in}},$$

where $\mathcal{G} > 1$ denotes the gain of the amplifier. As is evident, such scattering is symmetric between signal and idler. Breaking this symmetry and realizing directional amplification is of immediate relevance to multiple quantum-information-processing (QIP) platforms, as it would (i) ensure unidirectional information transfer, (ii) prevent any noise impinging on the output port from getting amplified and redirected to the signal source (such as qubits), and (iii) significantly simplify measurement chains by eliminating the need for bulky components such as circulators and isolators, ultimately paving the way towards fully integrated QIP.

It is worth noting that ideal directionality, while remaining strictly confined to two modes,

$$\begin{pmatrix} a_{\mathrm{sig}} \\ a_{\mathrm{idl}} \end{pmatrix}^{\mathrm{out}} = \begin{pmatrix} 0 & 0 \\ \sqrt{\mathcal{G}} & \sqrt{\mathcal{G}+1} \end{pmatrix} \begin{pmatrix} a_{\mathrm{sig}} \\ a_{\mathrm{idl}} \end{pmatrix}^{\mathrm{in}},$$

is forbidden by the requirement of a symplectic structure of scattering [4]. Thus, the challenge is to nonreciprocally transfer and amplify signals while introducing a minimum number of additional modes and preserve the quantum-limited operation of the device. Given the application potential of such systems, recent years have witnessed a strong surge in theoretical [5–10] and experimental [11–14] studies of quantum-limited nonreciprocity spanning acoustic, microwave, and optical frequencies.

In this work, we analyze nonreciprocal photon dynamics in a framework that emphasizes minimality of the mode space and parametric pumping—a feature especially desirable for hardware-efficient and scalable implementations of such detection protocols. Considering a generic system of three parametrically coupled bosonic modes, which is the natural next step in increased mode complexity, we show how a two-pump biharmonic drive of the form

$$G(t) = G_{\omega_p}\cos(\omega_p t) + G_{2\omega_p}\cos(2\omega_p t + \alpha) \qquad (1)$$

suffices to achieve various kinds of nonreciprocal couplings. Such biharmonic drives ($\alpha \neq n\pi$) are an economical way to realize time-asymmetric driving—this has been exploited to various ends previously, for instance,

 © 2017 American Physical Society

noise-induced ratchet dynamics in Brownian motors [15], the directed diffusion of cold atoms in optical lattices [16], the manipulation of fluxon transport in annular Josephson junctions [17], and the asymmetric driving of Landau-Zener-Stückelberg-Majorana interferences in double-quantum dots [18] and superconducting qubits [19]. An additional advantage associated with using biharmonic drives is their autonomous generation in nonlinear optical crystals [20] and Josephson junctions in the voltage state [21].

The paper is organized as follows. In Sec. II, we describe directional phase-preserving amplification in an alternative class of amplifiers which we call biharmonic Raman amplifiers. We present calculations for both unresolved- and resolved-sideband regimes, and we compare the available directionality with each under the inclusion of relevant frequency-dependent nonresonant corrections. In Sec. III, we describe directional phase-sensitive amplification with a biharmonically pumped three-mode system. In Sec. IV, we discuss generic behavior and trade-offs concerning gain, bandwidth, and directionality. We also establish the connection of biharmonic pumping schemes to recently proposed dissipation engineering frameworks [9], and we show that the general recipe of balancing dissipative and coherent interactions for implementing nonreciprocity simply maps to tuning the amplitude ratio $(G_{2\omega_p}/G_{\omega_p})$ and phase difference (α) of the two pump harmonics. We end the discussion with pointers for experimental designs based on the schemes presented in Secs. II and III. We conclude with a summary of our results in Sec. V. Additional details are included in Appendixes A, B, and C. Note, in this paper, we have used square brackets for frequency arguments in all equations and text; parentheses are used for time arguments.

II. DIRECTIONAL PHASE-PRESERVING AMPLIFICATION: BIHARMONIC RAMAN AMPLIFIERS

Phase-preserving amplification refers to the equal amplification of both quadratures of a photonic field; this process maintains the phase information of the amplified signal in the quadrature space. Our general scheme for a directional version of such a process is best understood in the framework of stimulated Raman scattering. It involves using a pump tone that is blue detuned from the lower sideband, resulting in Stokes scattering of the pump photons, and red detuned from the upper sideband, leading to anti-Stokes scattering (see Fig. 1). While the single-pump Stokes and anti-Stokes scattering is symmetric, it has been shown previously that the addition of the second pump harmonic induces asymmetry in these conversion processes [21]. Here, we elaborate on how such a process leads to directional amplification in the reduced subspace of the two sidebands. The basic idea relies on balancing (or "interfering") an indirect interaction between the two sidebands mediated by the first pump harmonic (through a third auxiliary mode), with a direct coherent interaction between the sidebands mediated by the second pump harmonic. The indirect interaction mediated by the auxiliary mode models a dissipative interaction, as discussed in Sec. IV.

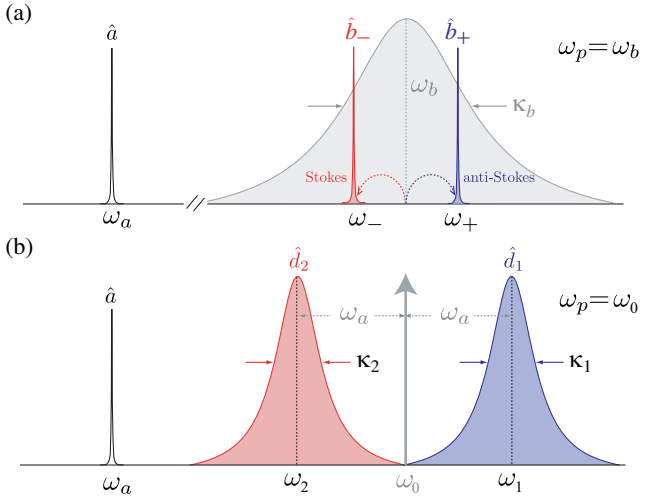

FIG. 1. Frequency landscape of Raman amplifiers in (a) an unresolved-sideband regime ($\kappa_a \ll \omega_a < \kappa_b$), and (b) a resolved-sideband regime ($\kappa_a \ll \kappa_{1,2} < \omega_a$). In both cases, the presence of an additional tone at $2\omega_p$ leads to directional amplification between $\omega_-(\omega_2)$ and $\omega_+(\omega_1)$.

We discuss two different regimes of these amplifiers:

(i) Unresolved-sideband amplification, i.e., $\omega_a \ll \kappa_b$, where κ_b denotes the linewidth of the high-frequency oscillator at ω_b and ω_a corresponds to the resonance frequency of the auxiliary mode [see Fig. 1(a)]. This regime corresponds to *degenerate phase-preserving amplification* since both input and output channels are accessed through a single oscillator [22].

(ii) Resolved-sideband amplification, i.e., $\omega_a \gg \kappa_b$. This regime corresponds to *nondegenerate phase-preserving amplification* since input and output channels are accessed via two distinct oscillators [see Fig. 1(b)].

A. Unresolved-sideband (USB) amplification

The Hamiltonian describing three bosonic modes coupled via time-varying (pairwise) interactions can be written

$$\hat{\mathcal{H}}_s = G_1(t)(\hat{a}+\hat{a}^\dagger)(\hat{d}_1+\hat{d}_1^\dagger) + G_2(t)(\hat{d}_1+\hat{d}_1^\dagger)(\hat{d}_2+\hat{d}_2^\dagger) + G_3(t)(\hat{a}+\hat{a}^\dagger)(\hat{d}_2+\hat{d}_2^\dagger), \quad (2)$$

where $\hat{a}$ $(\hat{d}_{1,2})$ denotes the photon annihilation operator of the mode with the frequency ω_a $(\omega_{1,2})$. The modulations $G_j(t)$ $(j \in 1;2;3)$ include the first and/or the second harmonic of an external pump at the frequency ω_p; see Eq. (1).

We first consider the scheme depicted in Fig. 1(a). This system, in principle, is a two-mode system and can be implemented using two parametrically coupled oscillators with the frequencies $\omega_{a,b}$. In the unresolved-sideband limit, where $\omega_a/\kappa_b \ll 1$, we can consider the low-frequency mode at ω_a and the two sidebands at $\omega_\pm = \omega_b \pm \omega_a$ as forming an effective three-mode system. Treating the sidebands as the independent modes $\hat{b}_\pm$, the system can be mapped to the general three-mode interaction Hamiltonian of Eq. (2) via the correspondence

$$\hat{d}_1 \to \hat{b}_+ = \hat{b}e^{i\omega_a t}, \qquad \hat{d}_2 \to \hat{b}_- = \hat{b}e^{-i\omega_a t}, \tag{3}$$

In the presence of a biharmonic drive of the form indicated in Eq. (1) and with $\omega_p = \omega_b$, the first pump harmonic induces Stokes (anti-Stokes) scattering to the lower (upper) sideband, while the second pump mediates a parametric-amplifier (paramp) interaction between the two sidebands since $2\omega_p = \omega_+ + \omega_-$. In an interaction picture, defined with respect to the free Hamiltonian of the two oscillators, these processes can be described by an effective mixing Hamiltonian of the form,

$$\begin{aligned}\hat{\mathcal{H}}_s = {} & G_1(\hat{a}e^{-i\omega_a t} + \hat{a}^\dagger e^{i\omega_a t})(\hat{b} + \hat{b}^\dagger) \\ & + \frac{G_2}{2}(\hat{b}\,\hat{b}\,e^{i\alpha} + \hat{b}^\dagger\hat{b}^\dagger e^{-i\alpha}).\end{aligned} \tag{4}$$

The first line in Eq. (4) describes up- and down-conversion processes between the low-frequency mode $\hat{a}$ and the sidebands of the high-frequency mode at $\omega_\pm = \omega_b \pm \omega_a$. The second line corresponds to an additional mixing pathway between these sidebands. This additional pathway allows for directional amplification within the sidebands by closing the interference loop in the frequency domain, with the loop phase entirely controlled through $\arg(G_2)$ here. Such interference of the frequency-mixing processes has been recently employed to propose asymmetric frequency conversion [21] and to explain directional amplification in microwave superconducting quantum-interference device (SQUID) amplifiers [7,8]. It is worthwhile to note here that, for $G_2 = 0$ and $\omega_P = \omega_b$—i.e., a monochromatic driving on resonance with the high-frequency mode—the system behaves as an effective two-mode phase-preserving amplifier which is not directional but still has the interesting property of having no gain-bandwidth limitation. The monochromatic driving scheme is closely related to a kind of recently introduced dissipative amplifier [23] (see Appendix A for further details).

Setting the coupling strengths of the two oscillators to the external input-output ports as $\kappa_{a,b}$, we use the standard input-output theory [24] to derive the Heisenberg-Langevin equations describing the dynamics of our system. To highlight the relevant features of this setup, we start by focusing on the zero-frequency case. Thus, the low-frequency mode is on resonance and has the stationary solution

$$\hat{a}[0] = -i\frac{2G_1}{\kappa_a}(\hat{b}[\omega_a] + \hat{b}^\dagger[\omega_a]), \tag{5}$$

where we neglect any noise contribution driving the low-frequency oscillator for simplicity. We see that the mode $\hat{a}$ is coupled to the two sidebands lying at $\pm\omega_a$ in this rotated frame. Correspondingly, the sidebands couple to $\hat{a}[0]$ and $\hat{a}^\dagger[2\omega_a]$. For $\omega_a \gg \kappa_a$, the processes mixing Stokes and anti-Stokes with $\hat{a}^\dagger[2\omega_a]$ can be ignored under a rotating-wave approximation in the $\hat{b}_\pm$ basis [25]. In this limit, the stationary solution for $\hat{a}[0]$ can be used to obtain the corresponding solutions for the sidebands,

$$\begin{aligned}\chi_+^{-1}\hat{b}[\omega_a] &= -\frac{2}{\sqrt{\kappa_b}}\hat{b}_{\rm in}[\omega_a] - \left(\mathcal{C} + i\frac{2G_2}{\kappa_b}e^{-i\alpha}\right)\hat{b}^\dagger[\omega_a], \\ \chi_-^{-1}\hat{b}^\dagger[\omega_a] &= -\frac{2}{\sqrt{\kappa_b}}\hat{b}^\dagger_{\rm in}[\omega_a] + \left(\mathcal{C} + i\frac{2G_2}{\kappa_b}e^{i\alpha}\right)\hat{b}[\omega_a],\end{aligned} \tag{6}$$

with the modified susceptibilities $\chi_\pm^{-1} = [1 \pm \mathcal{C} - i(2\omega_a/\kappa_b)]$ and the cooperativity $\mathcal{C} = 4G_1^2/(\kappa_a\kappa_b)$. The operators $\hat{b}_{\rm in}$ and $\hat{b}^\dagger_{\rm in}$ describe any input impinging on the sideband frequencies of the b mode, i.e., an input signal one wishes to amplify—or just thermal and vacuum fluctuations. Unlike the case of a single pump ($G_2 = 0$), there are differences in how each sideband couples to the other, as reflected by the asymmetries in the terms within parenthesis in Eq. (6). Moreover, this asymmetry is tunable with the phase α and the strength G_2 of the second pump. It is straightforward to see that, for

$$G_2 = \frac{\kappa_b}{2}\mathcal{C}, \qquad \alpha = -\frac{\pi}{2}, \tag{7}$$

$\hat{b}[\omega_a]$ decouples from the reduced system of the two sidebands. This decoupling results in a directional interaction, where $\hat{b}^\dagger[\omega_a]$ is influenced by $\hat{b}[\omega_a]$, but not vice versa.

In order to calculate the full nonreciprocal scattering matrix of the system, we use the standard input-output relation $\hat{o}_{\rm out} = \hat{o}_{\rm in} + \sqrt{\kappa_o}\hat{o}$, $(o \in a, b)$. Here, we include the fluctuations impinging on the low-frequency mode ($\hat{a}_{\rm in}$) as well, which we had neglected earlier. Then the zero-frequency scattering matrix in the basis $\hat{\mathbf{D}}[0] = [\hat{a}[0], \hat{b}[\omega_a], \hat{b}^\dagger[\omega_a]]^T$ becomes (for $\omega_a/\kappa_b \ll 1$)

$$\mathbf{s}[0] = \begin{pmatrix} -1 & \frac{i2\sqrt{\mathcal{C}}}{1-\mathcal{C}} & \frac{i2\sqrt{\mathcal{C}}}{1-\mathcal{C}} \\ \frac{i2\sqrt{\mathcal{C}}}{1+\mathcal{C}} & -\frac{1-\mathcal{C}}{1+\mathcal{C}} & 0 \\ \frac{-i2\sqrt{\mathcal{C}}}{1+\mathcal{C}} & -\frac{4\mathcal{C}}{1-\mathcal{C}^2} & -\frac{1+\mathcal{C}}{1-\mathcal{C}} \end{pmatrix}, \tag{8}$$

where $\hat{\mathbf{D}}_{\rm out}[0] = \mathbf{s}[0]\hat{\mathbf{D}}_{\rm in}[0]$. The diagonal elements of this matrix correspond to the reflection coefficients, while

the off-diagonal elements describe up-conversion from the low frequency to the sideband frequencies (s_{21}, s_{31}) and the reverse process of down-conversion (s_{12}, s_{13}). We will henceforth focus on the elements s_{23} and s_{32} that describe the directional amplification between the two sidebands. An input signal at the upper sideband shows up amplified at the lower sideband—i.e., it gets down-converted in frequency—while any input on the lower sideband never shows up at the higher sideband as $s_{23} = 0$. Note that, for $\alpha = \pi/2$, the situation is reversed—i.e., a signal is upconverted between the sidebands and amplified—but this reversal also leads to unwanted amplification of the reflected input signal.

The zero-frequency gain can be read off from Eq. (8) as

$$\mathcal{G}_0 \equiv |s_{32}[0]|^2 = \frac{16\mathcal{C}^2}{(\mathcal{C}^2-1)^2}, \tag{9}$$

which increases as $\mathcal{C} \to 1^-$. We note that stable operation of the amplifier requires $\mathcal{C} < 1$. From the second row of the scattering matrix, we also see that the reflection at the input vanishes (since $s_{22} = 0$) in the large gain limit, a feature desirable for applications such as qubit readout. Furthermore, the noise appearing at the input (upper sideband) stems from the low-frequency auxiliary mode alone. Moreover, the sideband amplification process described by Eq. (8) is quantum limited, as can be seen by calculating the total added noise at the output (lower sideband),

$$\overline{n}_{\rm add} = \frac{1}{2} + \overline{n}_b^T + \left(2\overline{n}_b^T + \overline{n}_a^T + \frac{3}{2}\right)\frac{1}{\mathcal{G}_0} + O\left(\frac{1}{\mathcal{G}_0^2}\right). \tag{10}$$

In the regime of large gain ($\mathcal{G}_0$) and zero-temperature baths ($\bar{n}_a^T = \bar{n}_b^T \approx 0$), we obtain the quantum limit of $\overline{n}_{\rm add} = 1/2$. Crucially, having a finite-temperature bath for the auxiliary mode, i.e., $\overline{n}_a^T > 0$, is not detrimental for the noise properties of the amplifier since the thermal-noise contribution of the auxiliary mode gets suppressed in the regime of large gain. This feature is especially valuable for an optomechanical setup where one utilizes a mechanical mode, with a significant thermal population, as the auxiliary mode. Similar noise suppression in reciprocal optomechanical-based amplifiers was found in Refs. [23,26] and was also reported in recent experiments [27,28].

Finally, we evaluate the expressions for the gain and the reverse gain as a function of frequency. We still consider the situation where the input signal injected at the upper sideband gets amplified and completely down-converted to the lower sideband under the directionality condition of Eq. (7). The finite frequency gain is ($\omega_a \ll \kappa_a$)

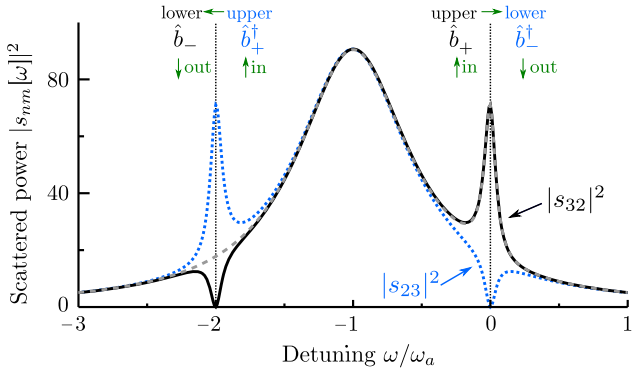

FIG. 2. Frequency dependence for the scattering-matrix elements of the unresolved-sideband amplification. The dashed gray line depicts the gain $|s_{32}[\omega]|$ under the rotating-wave approximation (RWA); see Eq. (11). The non-RWA results for forward and reverse gains are plotted as the solid black and dotted blue lines, respectively. The scattering-matrix elements at the sideband resonances $\omega_b \pm \omega_a$ describe down-conversion to the lower sideband for an input signal injected at the upper sideband. The parameters used in the calculation are $\mathcal{C} = 0.9$, $\omega_a/\kappa_b = 0.1$, $Q_a = 10$.

$$\mathcal{G}[\omega] = \frac{16\mathcal{C}^2\left(1+\frac{\omega^2}{\kappa_a^2}\right)\left(1+\frac{4\omega^2}{\kappa_a^2}\right)^{-1}}{\left[(\mathcal{C}-1)^2+\frac{4(\omega+\omega_a)^2}{\kappa_b^2}\right]\left[(\mathcal{C}+1)^2+\frac{4(\omega+\omega_a)^2}{\kappa_b^2}\right]}, \tag{11}$$

where the ratio of ω_a/κ_b is unspecified, i.e., the analysis is not restricted to the unresolved-sideband regime. The full expression for the frequency-dependent gain shows a peak at $\omega = -\omega_a$, which corresponds to the resonance frequency ω_b in the rotated frame (see Fig. 2). On the other hand, the reverse gain $\overline{\mathcal{G}}[\omega]$ describes the up-conversion of possible inputs, i.e., thermal or vacuum fluctuations from the lower sideband, and vanishes only at resonance ($\omega = 0$),

$$\overline{\mathcal{G}}[\omega] \equiv |s_{23}[\omega]|^2 = \frac{\frac{\omega^2}{\kappa_a^2}}{\left(1+\frac{\omega^2}{\kappa_a^2}\right)}\mathcal{G}[\omega]. \tag{12}$$

The ideal situation corresponds to a vanishing of the reverse gain over a wide frequency bandwidth. As is evident from Eq. (12), the range of signal frequencies for which the reverse gain can be suppressed increases with κ_a. However, treating both sidebands independently requires $\kappa_a \ll \omega_a$, i.e. a high-quality factor for the low-frequency $\hat{a}$ mode. One would think that having a large ω_a may do the trick for maintaining a large directionality bandwidth. However, just having a large ω_a is not sufficient, as, for $\omega_a \to \infty$, the gain vanishes as well. The relevant quantity here is the ratio ω_a/κ_b; this becomes obvious if we consider the gain at resonance [see Eq. (11)] for $\mathcal{C} \to 1^-$,

$$\mathcal{G}[0] = \frac{1}{\frac{\omega_a^2}{\kappa_b^2}\left(1+\frac{\omega_a^2}{\kappa_b^2}\right)} \approx \frac{\kappa_b^2}{\omega_a^2}. \tag{13}$$

The gain saturates and the maximal gain value scales with $(\kappa_b/\omega_a)^2$ for $\mathcal{C} \to 1^-$. Thus, the unresolved-sideband regime is an important ingredient to obtain any gain at all in the scheme.

B. Resolved-sideband (RSB) amplification

Our analysis in the previous section showed that the parameter hierarchy $\kappa_a \ll \omega_a < \kappa_b$ is crucial for directional phase-preserving amplification between the sidebands. The restriction to the unresolved-sideband regime, however, constrains both the forward gain and the directionality of such a biharmonic Raman amplifier. For instance, 20 dB of gain would already require a ratio of $\kappa_b/\omega_a \simeq 10$; though achievable in opto- and electromechanical setups, maintaining this ratio limits the application potential of such a scheme in superconducting setups employing microwave frequencies. In this section, we show how operating in the resolved-sideband regime alleviates these difficulties. We now extend our system to include three independent oscillators with resonance frequencies $\omega_a \ll \omega_2 < \omega_1$. As shown in Fig. 1(b), the independent modes at frequencies $\omega_{1,2}$ play the role of the sidebands of the USB amplifier case. Choosing the driving frequencies $\omega_{P,i}$, $[i \in (1,2,3)]$ of the time-dependent couplings $G_j(t)$ in Eq. (2) as

$$\omega_{P,1} = \omega_1 - \omega_a \equiv \omega_0, \tag{14a}$$

$$\omega_{P,2} = \omega_2 + \omega_a \equiv \omega_0, \tag{14b}$$

$$\omega_{P,3} = \omega_1 + \omega_2 \equiv 2\omega_0 \tag{14c}$$

makes the following interactions resonant in the system, just as in the unresolved-sideband regime:

(i) the first harmonic at ω_0 mediates a hopping interaction between the auxiliary mode $\hat{a}$ and the mode $\hat{d}_1$,
(ii) the first harmonic at ω_0 mediates an amplifier interaction between the auxiliary mode $\hat{a}$ and the mode $\hat{d}_2$, and
(iii) the second harmonic at $2\omega_0$ mediates an amplifier interaction between the modes $\hat{d}_2$ and $\hat{d}_1$.

As before, we work in an interaction picture with respect to the oscillators' free Hamiltonian and obtain

$$\hat{\mathcal{H}} = G_1(\hat{a}\hat{d}_1^\dagger + \hat{a}^\dagger\hat{d}_2^\dagger) + G_2\hat{d}_1^\dagger\hat{d}_2^\dagger e^{-i\alpha} + \hat{\mathcal{H}}_{\mathrm{CR}} + \mathrm{H.c.}, \tag{15}$$

where $\hat{\mathcal{H}}_{\mathrm{CR}}$ contains the counterrotating terms.

We consider the same situation as before, i.e., the directional amplification of an input signal at the upper mode with frequency ω_1 which shows up at the output of the mode at frequency ω_2. Using input-output theory and utilizing the directionality condition of Eq. (7), we obtain the same zero-frequency scattering matrix as in Eq. (8), but now in the basis $\hat{\mathbf{D}}[0] = [\hat{a}[0], \hat{d}_1[0], \hat{d}_2^\dagger[0]]^T$. The finite frequency gain for the RSB amplifier is given as (neglecting $\hat{\mathcal{H}}_{\mathrm{CR}}$)

$$\mathcal{G}[\omega] = \frac{16\mathcal{C}^2\left(1+\frac{\omega^2}{\kappa_a^2}\right)}{\left(1+\frac{4\omega^2}{\kappa_a^2}\right)\left[(\mathcal{C}-1)^2+\frac{4\omega^2}{\kappa_b^2}\right]\left[(\mathcal{C}+1)^2+\frac{4\omega^2}{\kappa_b^2}\right]}, \tag{16}$$

where, for simplicity, we assume equal decay rates for both oscillator mode 1 and oscillator mode 2, i.e., $\kappa_1 = \kappa_2 \equiv \kappa_b$. The reverse gain of the RSB amplifier is the same as that given in Eq. (12), with $\mathcal{G}[\omega]$ now given by Eq. (16). Thus, the situation is the same as that in the USB case; the reverse gain vanishes on resonance and the directionality bandwidth increases with κ_a. The important difference, however, is that the gain in Eq. (16) does not depend on the ratio ω_a/κ_b, in contrast to Eq. (11). Thus, there is no saturation of the gain, which limits the unresolved-sideband regime for large ω_a.

It is worthwhile to note that the directionality of the system is robust to pump detunings. Small pump detunings can be compensated for by detuning the input signal appropriately and accounting for an additional detuning-dependent phase shift between the pump harmonics (see Appendix B for details). We also discuss another mode of operation of this system—namely, a nonreciprocal photon transmission without gain or a frequency circulator—in Appendix C.

C. Influence of counterrotating terms: USB versus RSB

All of the calculations in previous sections are done while neglecting the counterrotating terms. These terms oscillate at 2 times one of the system frequencies, i.e., $e^{i2\omega_j t}$ $(j \in a,1,2,0)$; since the smallest frequency is ω_a, the terms oscillating at $2\omega_a$ are the most relevant counterrotating terms. Under this assumption, the counterrotating Hamiltonian can be written

$$\hat{\mathcal{H}}_{\mathrm{CR}} \simeq G_1(\hat{a}^\dagger\hat{d}_1^\dagger e^{i2\omega_a t} + \hat{a}\hat{d}_2^\dagger e^{-i2\omega_a t}) + \mathrm{H.c.} \tag{17}$$

Figure 3 compares the forward and reverse gains calculated, including the effect of Eq. (17), for both the USB and RSB types of biharmonic Raman amplifiers. It is clear that the counterrotating terms lower the forward gain of both amplifiers unless filtered out by a sufficiently high Q_a for the auxiliary mode, $\omega_a/\kappa_a \gg 1$. Furthermore, though a (reduced) forward gain persists in the low-Q_a regime, the reverse gain vanishes and directionality is restored only in the high-Q_a limit.

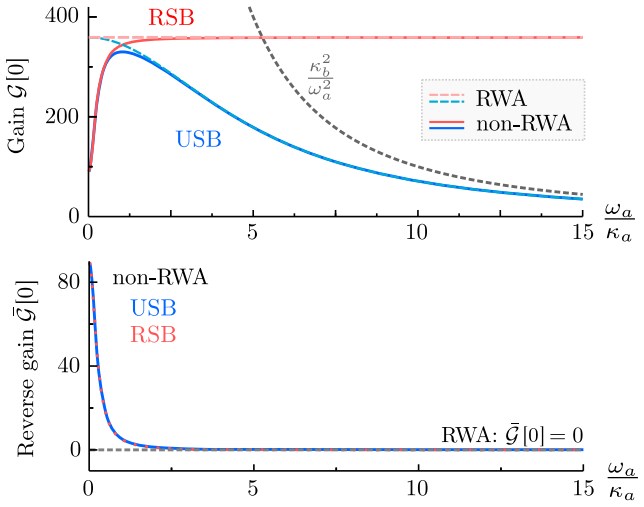

FIG. 3. Comparison of USB and RSB biharmonic Raman amplifiers for $\mathcal{C}=0.9$ and $\kappa_b=100\kappa_a$. The upper (lower) graph depicts the forward (reverse) gain at resonance, as a function of the quality factor of the auxiliary mode $Q_a=\omega_a/\kappa_a$. In the USB case, the gain first improves as Q_a increases and then decreases and reaches the limit κ_b^2/ω_a^2 (the gray dashed line) for a large Q_a. The RSB amplifier, on the other hand, suffers from no gain saturation and it operates at the expected maximal gain value, i.e., $\mathcal{G}\sim\mathcal{G}_0\approx 360$ for a high Q_a. Furthermore, inclusion of non-RWA corrections shows that $\omega_a>\kappa_a$ is necessary to suppress reverse gain in both the USB and RSB schemes (under a RWA, the reverse gain is always zero).

While the behaviors of the RSB amplifier and the USB amplifier coincide in the low-Q_a regime, the gain for the USB amplifier decreases strongly with an increasing Q_a. The saturation of the gain sets in as $\omega_a/\kappa_a\to\kappa_b/\kappa_a$ [see Eq. (13)], significantly limiting the useful bandwidth over which it can be exploited as a *directional* phase-preserving amplifier. Operating in the RSB regime alleviates this problem and drastically increases the bandwidth over which the amplifier is directional, though it still requires a modest Q_a for the auxiliary mode.

We revisit the bandwidth and directionality dependence on κ_a in detail in Sec. IV.

III. DIRECTIONAL PHASE-SENSITIVE AMPLIFICATION

We now present a biharmonically pumped three-mode scheme for directional phase-sensitive amplification. This system selects only one of the input quadratures which appears amplified at the output port, while the reverse process is completely suppressed. Originally proposed in Ref. [9], the key idea here is to design a quantum nondemolition (QND) interaction between the input and output modes. In the most general case, at least six driving tones are required to mediate the requisite interactions. In this section, we show how such an interaction can be implemented using a biharmonic tone, with only a single constraint on the auxiliary-mode frequency ω_a being degenerate with one of the input or output modes. To this end, we consider the most general three-mode Hamiltonian of Eq. (2) under the pumping conditions

$$\omega_1+\omega_a\equiv 2\omega_0,\qquad \omega_1-\omega_a=\omega_0 \tag{18a}$$

$$\omega_1+\omega_2\equiv 2\omega_0,\qquad \omega_1-\omega_2=\omega_0 \tag{18b}$$

$$\omega_2+\omega_a\equiv \omega_0,\qquad \omega_2-\omega_a=0, \tag{18c}$$

which selects the following interactions to be resonant:

(i) the first harmonic at ω_0 mediates a hopping interaction, while the second harmonic mediates a paramp interaction between the auxiliary mode $\hat{a}$ and the mode $\hat{d}_1$,

(ii) the first harmonic at ω_0 mediates a hopping interaction, while the second harmonic mediates a paramp interaction between modes $\hat{d}_1$ and $\hat{d}_2$, and

(iii) the first harmonic at ω_0 mediates a paramp interaction between the auxiliary mode $\hat{a}$ and the mode $\hat{d}_2$.

This pumping scheme can be easily realized for any combination of mode frequencies of the form $\omega_a=\omega_2=(1/3)\omega_1$. Note that the interaction between the auxiliary mode and mode 2 can only be of the amplifying type in this case since these modes are designed to be at the same frequency. Section IV presents a practical implementation of this idea utilizing a Josephson-junction-based mixing circuit (see Fig. 7).

The pump frequencies in Eq. (18) select the following interactions to be resonant:

$$\hat{\mathcal{H}}=G\hat{X}_1\hat{X}_2-G_3(\hat{X}_2\hat{V}+\hat{P}_2\hat{U})+G\hat{X}_1\hat{U}, \tag{19}$$

with $\hat{X}_i=(\hat{d}_i+\hat{d}_i^\dagger)/\sqrt{2}$, $\hat{P}_i=-i(\hat{d}_i-\hat{d}_i^\dagger)/\sqrt{2}$, $(i\in 1,2)$ being the quadratures associated with the input-output modes, and $(\hat{U},\hat{V})$ the quadratures associated with the auxiliary mode. Here, we have chosen $G_1=G_2\equiv G/2$ and the phase difference between G and G_3 to be $\pi/2$ [see Eq. (2)]. Equation (19) shows that $\hat{X}_1$ is a QND observable and is, therefore, preserved from quadrature mixing, as is desired for phase-sensitive amplification.

In the optimal case, $\hat{X}_2$ would also be a QND observable [9]; this scenario can be accomplished by balancing out the term $\hat{P}_2\hat{U}$ either through a static coupling [11] between modes $\hat{a}$ and $\hat{d}_2$ or by lifting their degeneracy at the expense of introducing additional pumps. Figure 4 illustrates the information transfer mediated by the Hamiltonian in Eq. (19). The information in the X quadratures of each mode is transferred to the respective P quadratures of the other mode in two ways: via a direct transfer and via a transfer through the auxiliary mode.

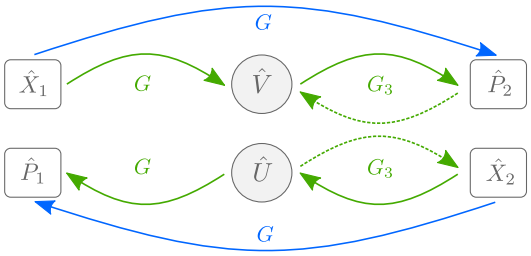

FIG. 4. The direct interaction between modes 1 and 2 (the solid blue curves) alone corresponds to an information transfer where the information of the X quadrature of each mode is dumped into the P quadrature of the respective opposite mode. The coupling to the auxiliary mode breaks this reciprocal process by mediating the same transfer process between the modes (the solid green curves). Balancing these processes leads to a perfect decoupling of mode 1 from mode 2. The dashed lines show the feedback loops, which may be mitigated by an additional static coupling between the auxiliary mode and mode 2. However, as shown by the scattering analysis, they are not too damaging for the whole scheme to work.

Balancing these interactions optimally leads to unidirectional information transfer between the selected input and output quadratures. This result can be easily seen from the zero-frequency scattering matrix calculated from the coupled equations of motion for the quadratures which, after the elimination of auxiliary mode, reads

$$\mathbf{s}[0] = \begin{pmatrix} -1 & 0 & 0 & 0 \\ 0 & -1 & 0 & 0 \\ 0 & 0 & -\frac{\kappa+\kappa_a}{\kappa-\kappa_a} & 0 \\ \frac{8G}{\kappa-\kappa_a} & 0 & 0 & -\frac{\kappa+\kappa_a}{\kappa-\kappa_a} \end{pmatrix} \tag{20}$$

in the basis $\hat{\mathbf{D}} = (\hat{X}_1, \hat{P}_1, \hat{X}_2, \hat{P}_2)^T$. Here, $\hat{\mathbf{D}}_{\text{out}} = \mathbf{s}\hat{\mathbf{D}}_{\text{in}} + \xi_a$ with ξ_a denoting the noise contribution from the auxiliary mode, and $\kappa_1 = \kappa_2 \equiv \kappa$. We also assume the optimal interaction strength to be $G_3 = \kappa_a/2$ to impose unidirectional coupling from mode 1 to mode 2. The process described by Eq. (20) is that of a directional phase-sensitive amplification, where $\hat{P}_{2,\text{out}}$ contains the amplified input quadrature $\hat{X}_{1,\text{in}}$, while no input in either of the mode-2 quadratures shows up at the output of mode 1. The amplitude gain scales with G and stability requires $\kappa_a \ll \kappa$, as the amplifier interaction between the auxiliary mode and mode 2 introduces antidamping of the latter. Moreover, the added noise

$$\overline{n}_{\text{add}} = \left(\frac{\kappa+\kappa_a}{8G}\right)^2 \left(\overline{n}_2^T + \frac{1}{2}\right) + \frac{\kappa_a \kappa}{16G^2}\left(\overline{n}_a^T + \frac{1}{2}\right) \tag{21}$$

goes to zero in the high-gain limit $G \gg \kappa, \kappa_a$ [see Fig. 5(c)], as desired for ideal phase-sensitive amplification. The expressions for frequency-dependent forward gain and reverse gain,

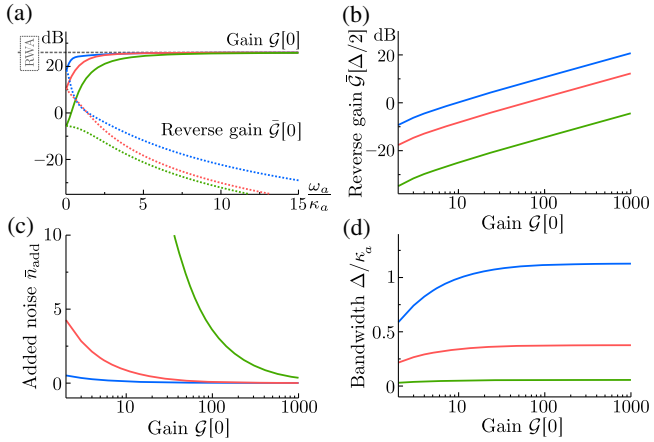

FIG. 5. Characteristics for the directional phase-sensitive amplifier scheme for three different ratio values of κ_a/κ: 0.1 (the blue curves), 0.5 (the red curves), 0.9 (the green curves). For each plot, the calculation assumes a directionality condition, namely, $G_3 = \kappa_a/2$. (a) Frequency-dependent forward and reverse gains as a function of $Q_a = \omega_a/\kappa_a$ for the auxiliary mode. The dashed gray line shows the gain without the counterrotating terms which is independent from Q_a, here $\mathcal{G}[0]^{\text{RWA}} = 26$ dB at resonance, while the corresponding reverse gain is always zero. For moderate quality factors, the reverse gain is highly suppressed, while the gain approaches the RWA result; hence, we chose $\omega_a/\kappa_a = 10$ for the calculations presented in (b)–(d). (b) Reverse gain evaluated at half of the amplification bandwidth, i.e., at $\omega = \Delta/2$, with Δ being the full width at half maximum of the forward-gain profile. (c) Added noise quanta versus zero-frequency gain for zero-temperature baths. (d) Amplification bandwidth expressed in units of the linewidth of the auxiliary mode, Δ/κ_a. Crucially, the bandwidth does not decrease while increasing the gain, leading to no gain-bandwidth limitation.

$$\mathcal{G}[\omega] = |s_{P_2 \leftarrow X_1}[\omega]|^2 = \frac{16\mathcal{C}_a\left(1+\frac{\omega^2}{\kappa_a^2}\right)}{\left(1+\frac{4\omega^2}{\kappa_a^2}\right)\left[\left(\frac{4\omega^2}{\kappa_a^2}+\frac{\kappa}{\kappa_a}-1\right)^2+\frac{4\omega^2}{\kappa_a^2}\left(1+\frac{\kappa}{\kappa_a}\right)^2\right]}, \tag{22}$$

$$\bar{\mathcal{G}}[\omega] = |s_{P_1 \leftarrow X_2}[\omega]|^2 = \frac{\frac{\omega^2}{\kappa_a^2}}{1+\frac{\omega^2}{\kappa_a^2}}\mathcal{G}[\omega], \tag{23}$$

where $\mathcal{C}_a = 4G^2/\kappa_a^2$. Crucially, the antidamping does not scale with the gain (though $\kappa_a < \kappa$), leading to no limitation on the gain-bandwidth product for this system.

Figure 5 depicts the relevant figures of merit for the directional phase-sensitive amplifier, calculated including the relevant next sideband contributions, i.e., counterrotating terms associated with $\omega_0 = 2\omega_b = 2\omega_a$ up to first order. Figure 5(a) shows that the auxiliary mode Q_a needs to be sufficiently high in order to obtain useful directionality; this finding coincides with the results found for phase-preserving amplification with biharmonic Raman amplifiers (see Fig. 3).

Furthermore, as shown by Figs. 5(c) and 5(d), for a given Q_a, having a too large κ_a is also detrimental from the point of view of the bandwidth and noise properties of such an amplifier. On the other hand, having a too small κ_a/κ ratio is unfavorable for directionality since the reverse gain is strongly suppressed only for a large κ_a/κ. Note that this ratio is always limited to less than unity due to stability considerations; this constraint arises due to the feedback of the quadrature mixing term $\hat{P}_2\hat{U}$ in Eq. (19). The desirable hierarchy of different frequency scales for stable directional operation thus becomes $\kappa_a < \kappa < \omega_a$.

IV. DISCUSSION

In this section, we discuss and highlight some common themes based on our results obtained for different biharmonic amplification schemes, and also comment on possible experimental adaptations.

A. Amplification bandwidth versus directionality bandwidth

The amplification bandwidth for biharmonic Raman amplifiers discussed in Sec. II can be calculated using the expression for forward gain [see Eq. (16)]. The forward gain is highest at the resonance of the selected mode and decreases with an increase in detuning as

$$\mathcal{G}[\omega]\underset{\mathcal{C}\to 1^-}{=}\mathcal{G}_0\frac{f(\vartheta_a)}{1+\mathcal{G}_0\vartheta_b^2}, \tag{24}$$

where $\vartheta_a = \omega/\kappa_a$, $\vartheta_b = (\omega+\omega_a)/\kappa_b$ for the USB amplifier and $\vartheta_{a,b} = \omega/\kappa_{a,b}$ for the RSB amplifier denote the respective reduced detunings. Here, we have retained only leading-order terms in ϑ_b. Also $f(\vartheta_a)$ denotes a polynomial function of ϑ_a which does not depend on the gain $\mathcal{G}_0$; hence it does not affect the gain-bandwidth product and can be taken as unity for $\vartheta_a \ll 1$. Equation (24) allows us to write the instantaneous amplification bandwidth as

$$\Delta(\mathcal{G}_0) \approx \frac{2\kappa_b}{\mathcal{G}_0^{1/2}}. \tag{25}$$

This trade-off between the maximum useful gain of an amplifier and the instantaneous bandwidth (or a constant gain-bandwidth product) is universal in most parametric-amplifier systems [29,30]. The directional phase-sensitive amplifier, on the other hand, shows no gain-bandwidth trade-off, as shown in Fig. 5(d) [see Eq. (22)].

To quantify the *directionality bandwidth* of the amplifiers presented in this work, we introduce a directionality parameter [see Eq. (12)]

$$d[\omega] \equiv 1-\frac{\overline{\mathcal{G}}[\omega]}{\mathcal{G}[\omega]} = \frac{1}{1+\vartheta_a^2}, \tag{26}$$

with $d=0$ corresponding to the usual reciprocal or symmetric amplification and $d=1$ corresponding to perfect nonreciprocity. Using a rationale similar to that employed while writing Eq. (24) allows us to infer the directionality bandwidth as

$$\Delta_d = 2\kappa_a. \tag{27}$$

It is straightforward to see that $\Delta_d/2$ denotes the detuning from resonance at which the directionality parameter reduces to $d=0.5$—i.e., a detuning that corresponds to a 3-dB isolation between the forward gain $\mathcal{G}[\omega]$ and the reverse gain $\overline{\mathcal{G}}[\omega]$. Crucially, directionality bandwidth Δ_d is independent of amplification bandwidth Δ, a behavior generic to these three-mode directional amplifiers. This fact is further borne out by the following observations:

(i) Equation (26) and, by consequence, Eq. (27) hold true for both phase-preserving and phase-sensitive operations, which show qualitatively different amplification-bandwidth behavior.

(ii) Unlike Δ, Δ_d is not limited by the gain $\mathcal{G}_0$ or by the linewidth κ_b of the amplified or deamplified mode, and it strictly scales with the linewidth of the auxiliary mode alone.

Therefore, in order to have directionality over a large bandwidth, it is essential for the auxiliary mode to have a proportionately large resonance linewidth κ_a. However, as shown by the results presented in Fig. 6, for both the phase-preserving and phase-sensitive amplifiers, the net achievable directionality d and directionality bandwidth deteriorate for a κ_a that is too large ($Q_a \to 0$). Specifically, for the case of a phase-preserving amplification, we find the simple scaling

$$d_{\mathrm{CR}}[0] = \frac{1}{1+\frac{1}{64Q_a^2}}, \tag{28}$$

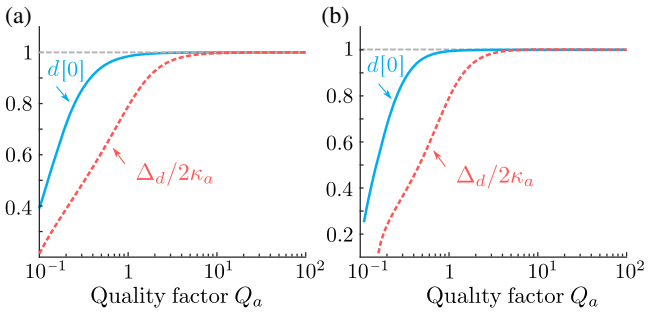

FIG. 6. Variation of directionality parameter at resonance $d[0]$ (the solid cyan curves) and directionality bandwidth Δ_d (the dashed red curves), with the quality factor Q_a of the auxiliary mode for (a) biharmonic Raman amplifiers and (b) a directional phase-sensitive amplifier. Both plots are calculated including the counterrotating terms, for a forward gain of $\mathcal{G} = 20$ dB.

which shows that the amplifier becomes reciprocal in the limit $Q_a \to 0$. Thus, the realization of directionality in the minimal three-mode schemes is predicated on a modestly high quality factor for the engineered reservoir mode, required to suppress the deleterious counterrotating contributions. Note that, while a directionality parameter of unity can be achieved at resonance ($\omega = 0$), the maximum attainable value of d decreases quadratically with detuning, as per Eq. (26). Also, the effect of non-RWA corrections is more pronounced at finite detunings.

A useful framework for distinguishing the effects of auxiliary-mode dynamics is to view this mode as an engineered reservoir, as is elaborated on in the following section.

B. Connection to dissipation engineering

It was recently shown that any factorizable coherent interaction can be rendered directional by balancing it with the corresponding dissipative interaction [9,31]. Dissipation is, therefore, the crucial element for obtaining any directionality at all. This contention also holds true for both phase-preserving and phase-sensitive biharmonic amplifier schemes, as described briefly in this section.

We start out from the Hamiltonian in Eq. (15), describing a hopping (paramp) interaction between the upper (lower) sideband mode and the low-frequency mode, as well as mixing between the two sidebands mediated by the second harmonic. The auxiliary mode $\hat{a}$ can be considered the engineered reservoir that provides us with the desired dissipative interaction. Elimination of this mode leads to the following coupled equations for the remaining modes 1 and 2:

$$\begin{aligned}\hat{d}_1[\omega] &\sim -i\left[\tilde{G}_2[\omega] - i\frac{\Gamma[\omega]}{2}\right]\hat{d}_2^\dagger[\omega],\\ \hat{d}_2^\dagger[\omega] &\sim +i\left[\tilde{G}_2^*[\omega] - i\frac{\Gamma[\omega]}{2}\right]\hat{d}_1[\omega].\end{aligned} \tag{29}$$

Here, we consider the full frequency dependence of the auxiliary mode and, accordingly, define the couplings

$$\tilde{G}_2[\omega] = G_2 e^{-i\alpha} + \frac{\frac{\omega}{\kappa_a}\Gamma_0}{1+\frac{4\omega^2}{\kappa_a^2}}, \qquad \Gamma[\omega] = \frac{\Gamma_0}{1+\frac{4\omega^2}{\kappa_a^2}}, \tag{30}$$

with $\Gamma_0 = 4G_1^2/\kappa_a$. The first term in each part of Eq. (29) corresponds to a coherent interaction and can be obtained from an effective Hamiltonian of the form $\mathcal{H}_{\rm coh} = \tilde{G}_2[\omega]\hat{d}_1^\dagger\hat{d}_2^\dagger + \text{H.c.}$ The same does not hold true for the second coupling term, which is impossible to obtain from a unitary interaction between $\hat{d}_1$ and $\hat{d}_2$. These terms correspond to a dissipative interaction mediated by the auxiliary mode, i.e., they could be derived from an effective nonlocal dissipator $\Gamma[\omega]\mathcal{L}[\hat{d}_1 + \hat{d}_2^\dagger]\hat{\rho}$ in a master equation [32].

The general condition of balancing a coherent interaction with its dissipative counterpart reported in Ref. [9] translates into simply tuning the amplitude and the phase of the coherent coupling,

$$|\tilde{G}_2[\omega]| = \frac{\Gamma[\omega]}{2}, \qquad \arg\left[\tilde{G}_2[\omega]\right] = \pm\frac{\pi}{2}. \tag{31}$$

Applying these conditions to Eq. (29) renders the coupling between the two modes directional. This selective decoupling would not be possible without the dissipative interaction. In principle, the system could be rendered directional for every frequency with the above conditions. However, in an experiment, the amplitude G_2 and the phase α will be fixed and the system is rendered completely directional at a single frequency; e.g., in the present frame, this circumstance would be at resonance, i.e., $\omega = 0$. The frequency range around that frequency over which the reverse gain is suppressed is then determined by κ_a, i.e., the inverse memory time of the engineered reservoir, as explained in the previous section. If this memory time is vanishingly small, i.e., the auxiliary mode $\hat{a}$ is strongly damped, then it can be treated as a Markovian reservoir and the whole system can be modeled via a Lindblad master equation of the form

$$\frac{d}{dt}\hat{\rho} = -i[\mathcal{H}_{\rm coh}, \hat{\rho}] + \Gamma_0\mathcal{L}[\hat{d}_1 + \hat{d}_2^\dagger]\hat{\rho}. \tag{32}$$

Here, the nonlocal dissipator describes a Markovian reservoir which absorbs excitation from mode $\hat{d}_1$ and emits it into $\hat{d}_2^\dagger$, with a rate Γ_0. In the overdamped case, the master equation sufficiently describes the system. For an arbitrary damping constant κ_a, a full description of the amplification dynamics needs to include the non-Markovian effects due to the finite lifetime of the reservoir (i.e., the low-frequency mode in this work).

C. Experimental implementations

We now discuss some pointers for practical designs based on the minimal schemes discussed here. Specifically, we comment on the prospects and challenges associated with implementations employing superconducting circuits and optomechanical systems—two platforms which have recently witnessed a lot of activity in nonreciprocal systems.

The two primary considerations for successful design include (i) strong parametric (nonlinear) coupling and (ii) low thermal population for the reservoir or auxiliary mode. While the strong parametric coupling is required to implement efficient pumping by the pump harmonics, a low auxiliary population is necessary to attain quantum-limited added noise. Three-wave mixers based on superconducting microwave circuits, such as the Josephson parametric converter (JPC) [33], are poised to exploit the biharmonic pump-mediated directionality. Figure 7 shows one such

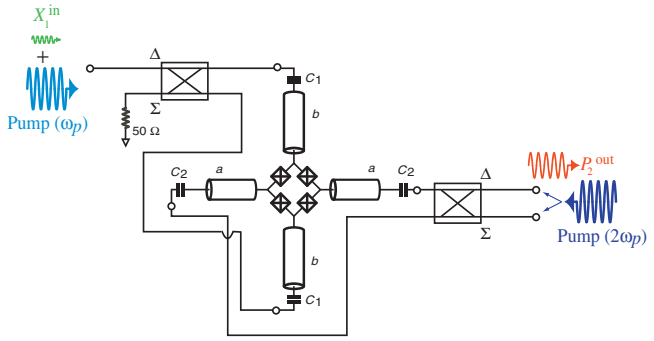

FIG. 7. Implementation of a directional phase-sensitive amplifier using a Josephson parametric converter (JPC) showing the signal and the pump waves. Here the X, Y, and Z modes of the JPC address the signal output, the signal input, and the auxiliary modes of the amplifier, respectively.

scheme that realizes the phase-sensitive amplifier presented in Sec. III. Here, the strong nonlinearity of the JPC at the few-quanta level and the concomitant parametric-coupling strength (approximately 1 MHz) [29] enable off-resonant driving mediated by the second pump harmonic. In addition, the residual thermal population in microwave resonators is negligible at typical dilution-refrigeration temperatures of tens of millikelvins, as shown in both 2D [34,35] and 3D geometries [36].

For optomechanical systems, the primary challenge is to realize strong coupling with the mechanical mode. Nonetheless, recent experiments have shown progress in this direction and have achieved optomechanical coupling strengths in the submegahertz (0.5–1.0 MHz) range [37]. Combined with the large dynamic range or photon processing power available with these systems, the resultant large multiphoton cooperativity should enable efficient mixing and mediate off-resonant parametric processes. Another promising direction is interfacing the mechanical modes with nonlinear microwave circuits that leverage the large nonlinearity of a Josephson junction. A single-photon coupling strength of $g_0 > 1$ MHz was recently demonstrated in a cavity-optomechanical system with a mechanically compliant superconducting charge qubit [38]; recent theoretical estimates predict a g_0 in excess of 100 MHz for such hybrid schemes [39]. Furthermore, suppression of thermal noise and quantum-limited behavior have also been demonstrated in cavity-optomechanical amplifiers [see Eq. (10) and the ensuing discussion], which makes them desirable platforms for biharmonic nonreciprocal amplifiers.

V. CONCLUSIONS

In this work, we study different modalities of directional quantum-limited amplification realizable in a three-mode system pumped with a biharmonic pump. For an optimal amplitude and phase difference between the two harmonics and an appropriate choice of mode frequencies, such a system provides the minimal implementation of nonreciprocal photon transmission and amplification. We present specific schemes for directional phase-preserving (both degenerate and nondegenerate) and directional phase-sensitive amplifications. The generality and minimality of our proposals should make them compatible with multiple platforms, such as superconducting qubits, nonlinear optical platforms, and opto- or electromechanical systems. Using pump harmonics can be particularly desirable in optical systems, where, supplemented by second- or subharmonic generation, it can drastically reduce the resource overhead in nonreciprocal optical platforms.

We also evaluate full frequency-dependent forward and reverse gains, and the available bandwidth with each scheme. Our results show that there is a universal separation of parameters determining directionality bandwidth and amplification bandwidth. Specifically, the directionality bandwidth increases directly with the linewidth of the dissipative or auxiliary mode alone. While it is desirable to have a fast auxiliary mode for stable device operation and large directionality bandwidth, inclusion of non-RWA corrections show that no net directionality is attainable if it is a very low-Q waveguide or a resistive mode.

ACKNOWLEDGMENTS

The authors wish to thank Aashish Clerk, Michel Devoret, Leonardo Ranzani, and John Teufel for the useful discussions. A. K. also acknowledges support from UMass Lowell start-up funds for this work.

APPENDIX A: SINGLE-PUMP RAMAN AMPLIFIER

We consider a single-pump modulation $M(t) = G(e^{-i\omega_p t} + e^{i\omega_p t})$ for the Raman amplifier in the unresolved-sideband regime [Fig. 1(a)], with $\omega_p = \omega_b$. Going into an interaction picture with respect to the free Hamiltonian, we obtain

$$\hat{\mathcal{H}}' = G_1(\hat{a}e^{-i\omega_a t} + \hat{a}^\dagger e^{i\omega_a t})(\hat{b} + \hat{b}^\dagger) + \hat{\mathcal{H}}_{\rm CR} + \hat{\mathcal{H}}'_{\rm bath}, \tag{A1}$$

with the counterrotating terms

$$\hat{\mathcal{H}}_{\rm CR} = G_1(\hat{b}e^{-i2\omega_b t} + \hat{b}^\dagger e^{i2\omega_b t})(\hat{a}e^{-i\omega_a t} + \hat{a}^\dagger e^{i\omega_a t}). \tag{A2}$$

Ignoring the counterrotating terms under the assumption of a high Q_a for the low-frequency oscillator, i.e., $\kappa_a \ll \omega_a < \kappa_b$, the zero-frequency scattering matrix can be approximated as

$$\mathrm{s}[0] \approx \begin{pmatrix} -1 & 2i\sqrt{\mathcal{C}} & 2i\sqrt{\mathcal{C}} \\ 2i\sqrt{\mathcal{C}} & (2\mathcal{C}-1) & 2\mathcal{C} \\ -2i\sqrt{\mathcal{C}} & -2\mathcal{C} & -(2\mathcal{C}+1) \end{pmatrix}, \tag{A3}$$

where $\hat{\mathbf{D}}_{\rm out}[0] = \mathrm{s}[0]\hat{\mathbf{D}}_{\rm in}[0]$, with $\hat{\mathbf{D}}_{\rm in}[0] = (\hat{a}_{\rm in}[0], \hat{b}_{\rm in}[\omega_a], \hat{b}^\dagger_{\rm in}[\omega_a])^T$, and cooperativity $\mathcal{C} = 4G_1^2/(\kappa_a\kappa_b)$.

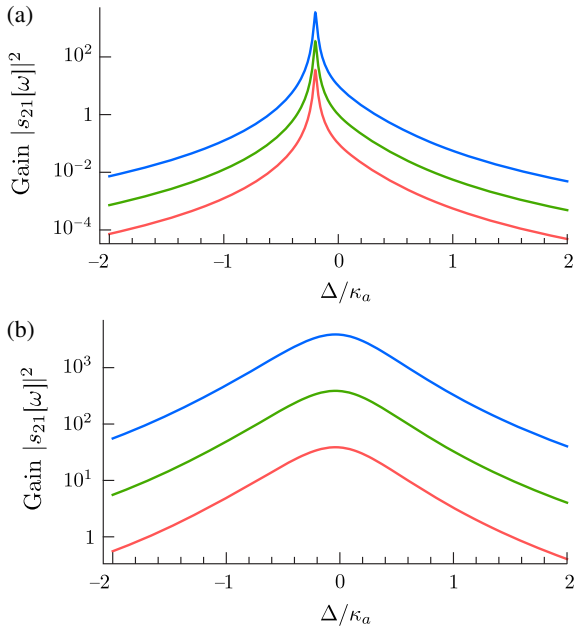

FIG. 8. Gain profiles of a single-pump Raman amplifier calculated for (a) $\omega_a/\kappa_a = 10$, $\omega_a/\kappa_b = 0.2$ and (b) $\omega_a/\kappa_a = 0.1$, $\omega_a/\kappa_b = 0.2$, with three values of cooperativity $\mathcal{C}$: 10 (the red curves), 100 (the green curves), 1000 (the blue curves). Note here that, due to the absence of any instability in the system, the cooperativity $\mathcal{C}$ does not need to be limited to a value less than unity.

Note that, in the absence of the second harmonic, the scattering is reciprocal. The expression for the frequency-dependent intermodulation gain between the modulation frequency ω_a and the sidebands $\omega_\pm$ for this case is given by

$$|s_{21}[\omega]|^2 = \frac{4\mathcal{C}}{\left(1+\frac{4\omega^2}{\kappa_b^2}\right)\left[1+\frac{4(\omega+\omega_a)^2}{\kappa_a^2}\right]}. \tag{A4}$$

As shown in Fig. 8, the bandwidth does not shrink with an increasing gain, unlike the usual parametric amplification schemes. Also, the bandwidth scales as $\min[\kappa_a, \kappa_b]$.

The transmission power gain $|s_{21}[\omega]|^2$ is associated with a frequency-conversion process, i.e., a signal injected at the low-frequency mode will be upconverted to the lower sideband frequency. However, the system works as an amplifier without any frequency conversion in reflection as well, which means that a signal injected on either sideband is reflected with the amplitude gain $2\mathcal{C}-1$. Such a phase-sensitive amplifier has been demonstrated experimentally [40] and has a close connection to the dissipative amplifier discussed in Ref. [23]. This connection becomes obvious if we use the mapping defined in Eq. (3) in Eq. (A1), which yields an interaction,

$$\hat{\mathcal{H}} = G_1\hat{a}(\hat{b}_+^\dagger + \hat{b}_-) + \text{H.c.}, \tag{A5}$$

corresponding to a hopping (amplifier) interaction between the low-frequency mode and the upper (lower) sideband. Elimination of the low-frequency mode leads to a coupling between the modes that could be achieved not via a coherent interaction but by a nonlocal dissipator of the form $\mathcal{L}[\hat{b}_+^\dagger + \hat{b}_-]\hat{\rho}$.

Clearly, the same "dissipative" amplifier could be realized in the resolved-sideband regime, i.e., with two independent modes, $\hat{d}_1$ and $\hat{d}_2$. Based on such a three-mode setup, a recent experiment showed that broadband amplification close to the quantum limit is possible [27].

APPENDIX B: INFLUENCE OF PUMP DETUNINGS ON RSB AMPLIFICATION

In Sec. II B, we focus on the somewhat ideal situation that the drive is exactly at ω_0. Here, we discuss the consequences of pump detuning from the frequencies noted in Eq. (14). We retain the assumption that the resonances at $\omega_{1,2}$ are perfectly tuned by design, i.e., exactly $2\omega_a$ apart. This is not a restrictive assumption since the detuning of the resonator frequencies results in a situation analogous to the one discussed here for detuned pumps. For a pump detuning δ, the modified driving conditions read

$$\begin{aligned}\omega_{P,1} &= \omega_0 + \delta = \omega_1 - \omega_a + \delta,\\ \omega_{P,2} &= \omega_0 + \delta = \omega_2 + \omega_a + \delta,\\ \omega_{P,3} &= 2(\omega_0+\delta) = \omega_1 + \omega_2 + 2\delta,\end{aligned} \tag{B1}$$

leading to the time-dependent interaction Hamiltonian

$$\hat{\mathcal{H}} = G_1(\hat{a}\hat{d}_1^\dagger e^{-i\delta t} + \hat{a}^\dagger\hat{d}_2^\dagger e^{-i\delta t}) + G_2\hat{d}_1^\dagger\hat{d}_2^\dagger e^{-i(2\delta t+\alpha)} + \text{H.c.} \tag{B2}$$

The corresponding equations of motion yield the coupling between mode 1 and mode 2 in the Fourier domain as

$$\begin{aligned}\hat{d}_1[\omega+\delta] &\sim -\left(\frac{2G_2}{\kappa_b}ie^{-i\alpha} + \frac{\mathcal{C}}{1-i\frac{2\omega}{\kappa_a}}\right)\hat{d}_2^\dagger[\omega-\delta],\\ \hat{d}_2^\dagger[\omega-\delta] &\sim +\left(\frac{2G_2}{\kappa_b}ie^{+i\alpha} + \frac{\mathcal{C}}{1-i\frac{2\omega}{\kappa_a}}\right)\hat{d}_1[\omega+\delta],\end{aligned} \tag{B3}$$

where we have eliminated the low-frequency mode, i.e., $\hat{a}[\omega]$. Similar to Eq. (29), the coupling is frequency dependent, but the modes do not couple exactly at their resonances. For example, $\hat{d}_1[0]$ couples to $\hat{d}_2^\dagger[-2\delta]$, i.e., to the field which is 2δ detuned from ω_2.

Crucially, the coupling between modes 1 and 2 can be made directional at any frequency ω_{dir}. The general directionality conditions read

$$\frac{2G_2}{\kappa_b} = \frac{\mathcal{C}}{\sqrt{1+\frac{4\omega_{\text{dir}}^2}{\kappa_a^2}}}, \qquad \alpha = -\frac{\pi}{2} - \arctan\left(\frac{2\omega_{\text{dir}}}{\kappa_a}\right). \tag{B4}$$

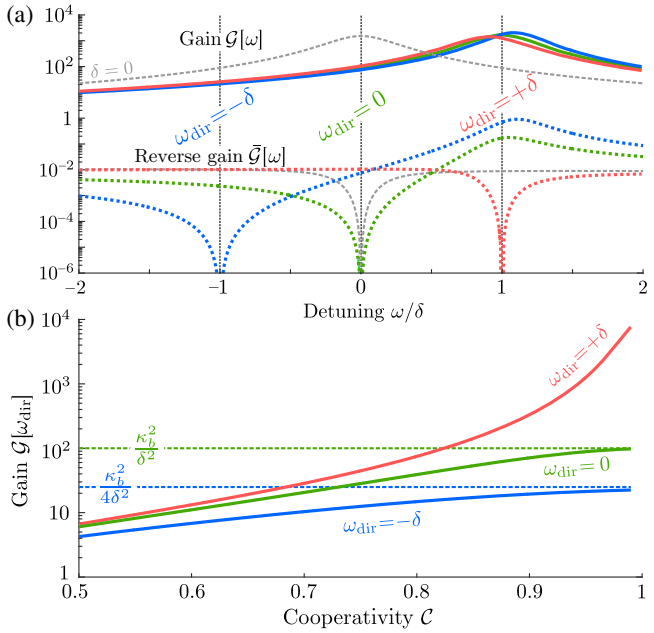

FIG. 9. Transmission properties of the RSB amplifier, in the presence of a finite pump detuning δ, calculated for $\delta/\kappa_b = 0.1$ and $\kappa_a/\kappa_b = 10$. (a) Gain (the solid curves) and reverse gain (the dashed curves) as a function of frequency for $\mathcal{C} = 0.95$ and three different choices of $\omega_{\rm dir}$. The reverse gain vanishes at the frequencies $\omega_{\rm dir} = 0, \pm\delta$ under the respective directionality condition in Eq. (B4). The overall magnitude of gain is only slightly affected due to the frequency-dependent variation of the effective couplings. (b) Gain maxima as a function of cooperativity. Only for $\omega_{\rm dir} = \delta$ does the gain not saturate.

It is straightforward to see that, for $\omega_{\rm dir} = 0$, we recover the directionality conditions from Eq. (7), resulting in the resonant gain,

$$\mathcal{G}[\omega = 0] = \frac{16\mathcal{C}^2}{(\mathcal{C}^2-1)^2 + (\mathcal{C}^2+1)\frac{8\delta^2}{\kappa_b^2} + \frac{16\delta^4}{\kappa_b^4}} \overset{\mathcal{C}\to 1}{\longrightarrow} \frac{\frac{\kappa_b^2}{\delta^2}}{1+\frac{\delta^2}{\kappa_b^2}}, \tag{B5}$$

while the reverse gain vanishes. It is important to note that the gain is suppressed in comparison to the case without any detuning and saturates around κ_b^2/δ^2 for a small detuning. Furthermore, for $\omega_{\rm dir} = 0$, the mode-1 input signal must be injected at $\omega_1 + \delta$, and the down-converted output signal appears at $\omega_2 + \delta$.

Similarly, we can consider an input exactly at the mode-1 resonance $\omega_{\rm dir} = -\delta$. Here, the input signal is down-converted to the frequency $\omega_2 + 2\delta$. The resulting gain in this case is even lower than that for the input at $\omega_{\rm dir} = 0$, and it saturates at $\kappa_b^2/4\delta^2$ [see Fig. 9(b)]. However, the reverse situation, $\omega_{\rm dir} = +\delta$ with the output appearing exactly at the mode-2 resonance, is most favorable. In this case, the input signal has to be injected 2δ detuned above the resonance frequency of mode 1, i.e., $\omega_1 + 2\delta$, while the output appears at ω_2 with a power gain

$$\mathcal{G}[\omega = +\delta] \approx \left[\frac{16\mathcal{C}^2}{(1+\mathcal{C})^2 + \frac{16\delta^2}{\kappa_b^2}}\right]\frac{1}{(1-\mathcal{C})^2}, \tag{B6}$$

which does not saturate and increases as $\mathcal{C} \to 1$.

APPENDIX C: GAINLESS CIRCULATION WITH A BIHARMONIC PUMP

The general three-mode interaction Hamiltonian in Eq. (2) can be tuned to realize a gainless nonreciprocal transmission between different channels, namely, a frequency circulator. This kind of system was recently discussed by Ranzani and Aumentado [8] and experimentally realized in a JPC setup [14]. These schemes require three pump tones which drive photon hopping between the three modes of the JPC described by the Hamiltonian,

$$\hat{\mathcal{H}} = G_1(\hat{a}\hat{d}_1^\dagger + \hat{a}\hat{d}_2^\dagger) + G_2\hat{d}_1\hat{d}_2^\dagger e^{-i\alpha} + \text{H.c.} \tag{C1}$$

The biharmonic version of this three-mode interaction can be realized by selecting the driving frequencies as

$$\begin{aligned}\omega_{P,1} &= \omega_1 - \omega_a \equiv 2\omega_0,\\ \omega_{P,2} &= \omega_2 - \omega_a \equiv \omega_0,\\ \omega_{P,3} &= \omega_1 - \omega_2 \equiv \omega_0,\end{aligned} \tag{C2}$$

which implies $\omega_a + \omega_1 = 2\omega_2$. For example, if one would work with the pump frequency $\omega_0/(2\pi) = 4$ GHz and the low-frequency mode at $\omega_a/(2\pi) = 1$ GHz, one would need to have $\omega_1/(2\pi) = 9$ GHz and $\omega_2/(2\pi) = 5$ GHz for the remaining two oscillators.

[1] E. Jeffrey, D. Sank, J. Y. Mutus, T. C. White, J. Kelly, R. Barends, Y. Chen, Z. Chen, B. Chiaro, A. Dunsworth *et al.*, Fast Accurate State Measurement with Superconducting Qubits, Phys. Rev. Lett. **112**, 190504 (2014).
[2] D. Riste, M. Dukalski, C. A. Watson, G. de Lange, M. J. Tiggelman, Y. M. Blanter, K. W. Lehnert, R. N. Schouten, and L. DiCarlo, Deterministic entanglement of superconducting qubits by parity measurement and feedback, Nature (London) **502**, 350 (2013).
[3] C. M. Caves, Quantum limits on noise in linear amplifiers, Phys. Rev. D **26**, 1817 (1982).
[4] Symplectic symmetry follows from the bosonic commutation relations, and the associated conserved quantity is the mode space of amplification.
[5] J. Koch, A. A. Houck, K. L. Hur, and S. M. Girvin, Time-reversal-symmetry breaking in circuit-QED-based photon lattices, Phys. Rev. A **82**, 043811 (2010).
[6] A. Kamal, J. Clarke, and M. H. Devoret, Noiseless nonreciprocity in a parametric active device, Nat. Phys. **7**, 311 (2011).

[7] A. Kamal, J. Clarke, and M. H. Devoret, Gain, directionality, and noise in microwave SQUID amplifiers: Input-output approach, Phys. Rev. B **86**, 144510 (2012).
[8] L. Ranzani and J. Aumentado, Graph-based analysis of nonreciprocity in coupled-mode systems, New J. Phys. **17**, 023024 (2015).
[9] A. Metelmann and A. A. Clerk, Nonreciprocal Photon Transmission and Amplification via Reservoir Engineering, Phys. Rev. X **5**, 021025 (2015).
[10] J. Kerckhoff, K. Lalumière, B. J. Chapman, A. Blais, and K. W. Lehnert, On-Chip Superconducting Microwave Circulator from Synthetic Rotation, Phys. Rev. Applied **4**, 034002 (2015).
[11] B. Abdo, K. Sliwa, L. Frunzio, and M. Devoret, Directional Amplification with a Josephson Circuit, Phys. Rev. X **3**, 031001 (2013).
[12] L. D. Tzuang, K. Fang, P. Nussenzveig, S. Fan, and M. Lipson, Non-reciprocal phase shift induced by an effective magnetic flux for light, Nat. Photonics **8**, 701 (2014).
[13] R. Fleury, D. L. Sounas, C. F. Sieck, M. R. Haberman, and A. Alù, Sound isolation and giant linear nonreciprocity in a compact acoustic circulator, Science **343**, 516 (2014).
[14] K. M. Sliwa, M. Hatridge, A. Narla, S. Shankar, L. Frunzio, R. J. Schoelkopf, and M. H. Devoret, Reconfigurable Josephson Circulator/Directional Amplifier, Phys. Rev. X **5**, 041020 (2015).
[15] P. Hänggi, F. Marchesoni, and F. Nori, Brownian motors, Ann. Phys. (Berlin) **14**, 51 (2005).
[16] M. Schiavoni, L. Sanchez-Palencia, F. Renzoni, and G. Grynberg, Phase Control of Directed Diffusion in a Symmetric Optical Lattice, Phys. Rev. Lett. **90**, 094101 (2003).
[17] A. V. Ustinov, C. Coqui, A. Kemp, Y. Zolotaryuk, and M. Salerno, Ratchetlike Dynamics of Fluxons in Annular Josephson Junctions Driven by Biharmonic Microwave Fields, Phys. Rev. Lett. **93**, 087001 (2004).
[18] F. Forster, M. Mühlbacher, R. Blattmann, D. Schuh, W. Wegscheider, S. Ludwig, and S. Kohler, Landau-Zener interference at bichromatic driving, Phys. Rev. B **92**, 245422 (2015).
[19] S. Gustavsson, J. Bylander, and W. D. Oliver, Time-Reversal Symmetry and Universal Conductance Fluctuations in a Driven Two-Level System, Phys. Rev. Lett. **110**, 016603 (2013).
[20] G. D. Boyd and D. A. Kleinman, Parametric interaction of focused Gaussian light beams, J. Appl. Phys. **39**, 3597 (1968).
[21] A. Kamal, A. Roy, J. Clarke, and M. H. Devoret, Asymmetric Frequency Conversion in Nonlinear Systems Driven by a Biharmonic Pump, Phys. Rev. Lett. **113**, 247003 (2014).
[22] M. H. Devoret and A. Roy, Introduction to parametric amplification of quantum signals with Josephson circuits, C.R. Phys. **17**, 740 (2016).
[23] A. Metelmann and A. A. Clerk, Quantum-Limited Amplification via Reservoir Engineering, Phys. Rev. Lett. **112**, 133904 (2014).
[24] B. Yurke, in *Quantum Squeezing*, edited by P. Drummond and Z. Ficek (Springer, New York, 2004), p. 53.
[25] This is equivalent to treating the two sidebands as independent modes.
[26] B. A. Levitan, A. Metelmann, and A. A. Clerk, Optomechanics with two-phonon driving, New J. Phys. **18**, 093014 (2016).
[27] C. F. Ockeloen-Korppi, E. Damskägg, J.-M. Pirkkalainen, T. T. Heikkilä, F. Massel, and M. A. Sillanpää, Low-Noise Amplification and Frequency Conversion with a Multiport Microwave Optomechanical Device, Phys. Rev. X **6**, 041024 (2016).
[28] C. F. Ockeloen-Korppi, E. Damskägg, J.-M. Pirkkalainen, T. T. Heikkilä, F. Massel, and M. A. Sillanpää, Noiseless quantum measurement and squeezing of microwave fields utilizing mechanical vibrations, Phys. Rev. Lett. **118**, 103601 (2017).
[29] B. Abdo, A. Kamal, and M. Devoret, Nondegenerate three-wave mixing with the Josephson ring modulator, Phys. Rev. B **87**, 014508 (2013).
[30] C. Eichler and A. Wallraff, Controlling the dynamic range of a Josephson parametric amplifier, EPJ Quantum Techno. **1**, 2 (2014).
[31] A. Metelmann and A. A. Clerk, Nonreciprocal quantum interactions and devices via autonomous feedforward, Phys. Rev. A **95**, 013837 (2017).
[32] We use the definition $\mathcal{L}[\hat{o}]\hat{\rho} = \hat{o}\,\hat{\rho}\,\hat{o}^{\dagger} - 1/2\hat{o}^{\dagger}\hat{o}\,\hat{\rho} - 1/2\hat{\rho}\hat{o}^{\dagger}\hat{o}$.
[33] N. Bergeal, F. Schackert, M. Metcalfe, R. Vijay, V. E. Manucharyan, L. Frunzio, D. E. Prober, R. J. Schoelkopf, S. M. Girvin, and M. H. Devoret, Phase-preserving amplification near the quantum limit with a Josephson ring modulator, Nature (London) **465**, 64 (2010).
[34] F. Yan, S. Gustavsson, A. Kamal, J. Birenbaum, A. P. Sears, D. Hover, T. J. Gudmundsen, D. Rosenberg, G. Samach, S. Weber *et al.*, The flux qubit revisited to enhance coherence and reproducibility, Nat. Commun. **7**, 12964 (2016).
[35] A. Kamal, J. L. Yoder, F. Yan, T. J. Gudmundsen, D. Hover, A. P. Sears, P. Welander, T. P. Orlando, S. Gustavsson, and W. D. Oliver, Improved superconducting qubit coherence with high-temperature substrate annealing, arXiv:1606.09262.
[36] A. P. Sears, A. Petrenko, G. Catelani, L. Sun, H. Paik, G. Kirchmair, L. Frunzio, L. I. Glazman, S. M. Girvin, and R. J. Schoelkopf, Photon shot noise dephasing in the strong-dispersive limit of circuit QED, Phys. Rev. B **86**, 180504 (2012).
[37] K. Fang, J. Luo, A. Metelmann, M. H. Matheny, F. Marquardt, A. A. Clerk, and O. Painter, Generalized non-reciprocity in an optomechanical circuit via synthetic magnetism and reservoir engineering, Nat. Phys. doi:10.1038/nphys4009 (2017).
[38] J.-M. Pirkkalainen, S. U. Cho, F. Massel, J. Tuorila, T. T. Heikkilä, P. J. Hakonen, and M. A. Sillanpää, Cavity optomechanics mediated by a quantum two-level system, Nat. Commun. **6**, 6981 (2015).
[39] P. Arrangoiz-Arriola and A. H. Safavi-Naeini, Engineering interactions between superconducting qubits and phononic nanostructures, Phys. Rev. A **94**, 063864 (2016).
[40] J. Teufel (private communication).